Imperial College London
Department of Materials

# Characterisation Exercise Report

*Mervyn Ochoa-Dugoy*

Group: B17 CID: 02262227 Username: mo322

04 March 2024

## Abstract

Two unknown powdered samples A (white) and B (colourless) were characterised using Scanning Electron Microscopy (SEM), Transmission Electron Microscopy (TEM), Energy Dispersive X-ray spectroscopy (EDX), X-ray diffraction (XRD) and Fourier Transform Infrared Spectroscopy (FTIR) to identify the samples' constituent elements and their crystal structures. Both samples were discovered to be polymorphs of tetragonal titania, $TiO_2$, synthesized under different controlled conditions to transform anatase to rutile. Sample A's powder comprised of mixed rutile-anatase, 95.6 wt.% and 4.4 wt.% respectively, with high clustering platelets with an average single platelet at 0.47 ± 0.14 μm, as a result of sol-gel synthesis and calcination to elevated temperatures above 700°C, useful for protective surface coatings. Sample B saw a full transformation of 100% rutile $TiO_2$ from anatase, forming flower-like microparticles from nanorods, synthesised hydrothermally using $TiCl_4$ and prolonged mixing time. This included crystallite thicknesses in the (101) and (111) planes recording 12.51 nm and 11.47 nm respectively. Such microparticles improve efficiency for dye sensitised solar cells (DSSC's).

## Introduction*

Sample characterisation, crucial for understanding material processing and optimisation, employs techniques like SEM, TEM, XRD and EDX, enabling detailed analysis from atomic composition to crystal structures through high-magnification electron acceleration and X-ray diffraction[1]. This experiment aims to perform these techniques progressively and thoroughly analyse the produced results to encapsulate sample A and B's similarities and differences, leading to reasonable predictions to their processing.

## Materials and Methods

SEM, EDX and XRD were performed simultaneously for initial characterisation. A JEOL JSM-6010PLUS/LA 20kV was used for SEM and EDX, performed under a low vacuum setting. Both powdered samples A and B were spread out flat on the surface separately in individual stubs, supported by carbon tape and coated in gold (Au). The following magnifications were used on secondary electron mode (SEI): x50, x2000, x4000, x7000, x10000 and x20000 – with variant working distance and spot sizes (specified in Figure 4). Map EDX was taken at x50 and x4000 and point EDX was done at x7000 on both samples to qualitatively identify the elements involved.

XRD was then done using the Bruker D2 Phaser using a copper Kα source 30kV (of wavelength 1.541874 nm), 10mA and nickel filter. Both samples were placed on a zero-diffraction plate holder and inserted individually in the machine. The following scans were conducted using Bragg-Brentano geometry: sample A on 8-minute scan, 0.03° step size and sample B on 17 minutes, 0.02° step size. Results were plotted in real time by the Bruker software of intensity against 2θ, from 20° - 80°. To further characterise, TEM images were captured on sample B using the JEOL JEM-2100PLUS 200 kV microscope, using magnifications up to x600,000. ImageJ software was used to appropriately adjust brightness and contrast of the SEM and TEM images for improved visualisation on both samples[2]. Crystal Diffract Match! software identified the XRD peaks and compared patterns from Crystallography Open Database to verify the elements from EDX[3]. Scherrer analysis was conducted on Origin using the Lorentz peak fitting gadget to find the crystallite sizes of planes for both samples A and B[4].

## Results and Discussion

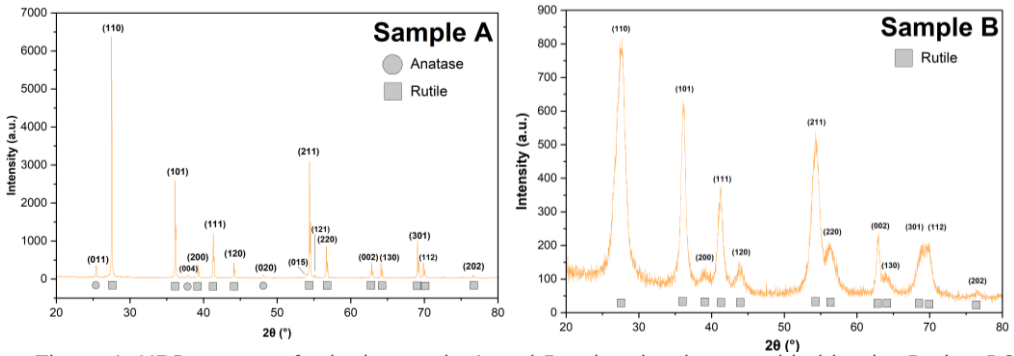


*Figure 1: XRD patterns for both sample A and B using the data provided by the Bruker D2 Phaser, scanning between 20° - 80°. Peaks were labelled with respect to the matching XRD patterns chosen by Match, including the characteristic planes for rutile and anatase $TiO_2$[3,5-7].*

| | | | SAMPLE A | | SAMPLE B | |
|---|---|---|---|---|---|---|
| Peak position (°) | (hkl) | Phase (A/R) | FWHM (rad) | Crystallite thickness (nm) | FWHM (rad) | Crystallite thickness (nm) |
| 25.40 | (011) | A | 0.105 | 77.80 | - | - |
| 27.52 | (110) | R | 0.092 | 88.65 | 1.49 | 5.59 |
| 36.15 | (101) | R | 0.095 | 87.64 | 0.70 | 12.51 |
| 37.89 | (004) | A | 0.091 | 92.35 | - | - |
| 39.18 | (200) | R | 0.091 | 92.30 | 1.32 | 6.39 |
| 41.27 | (111) | R | 0.095 | 89.55 | 0.74 | 11.47 |
| 43.98 | (120) | R | 0.091 | 94.74 | 1.64 | 5.35 |

*Table 2: Scherrer analysis for low angle 2θ values up to 45° of both sample A and B to determine their respective crystallite thicknesses (λ = 1.541874 nm, K = 0.9). Crystallite thickness and peak position values were rounded to 2 decimal places.*

Qualitatively in Figure 1, 17 peaks were observed in sample A, comparable to rutile and anatase (both tetragonal phases) in a 95.6-4.4 wt.% split, and 12 peaks were seen in sample B, composed of 100% rutile $TiO_2$ as matched by the Match! Crystal Open Database – with rutile's lattice parameters of a = 4.60 Å and c = 2.97 Å[5–7]. It was also evident that both samples were dominantly rutile, as the (110), (101) and (211) planes showed the highest intensity. The crystallite thicknesses were different in both samples using the Scherrer equation for low 2θ peaks - due to overlapping and Cu $K\alpha_2$ peaks, higher 2θ values were not analysed[8]. The calculated values in Table 2 saw that sample A had a low range of crystallite thicknesses between 77.80 to 92.35 nm implying isotropic growth in all orientations, therefore it can be averaged to 89.0 ± 4.8 nm – however further understanding of morphology will be required. Whereas for sample B, the (101) and (111) planes from Table 2 showed the highest crystallite sizes hinting anisotropic and preferential growth in these orientations. A higher background noise was observed for low 2θ in Figure 1 for sample B, which lowered values across all planes. It was likely from an instrumental setup error took place during the scan, such as sample preparation on the holder. Nevertheless, the pattern of results would still infer some other form of nanoscale morphology, different to sample A.

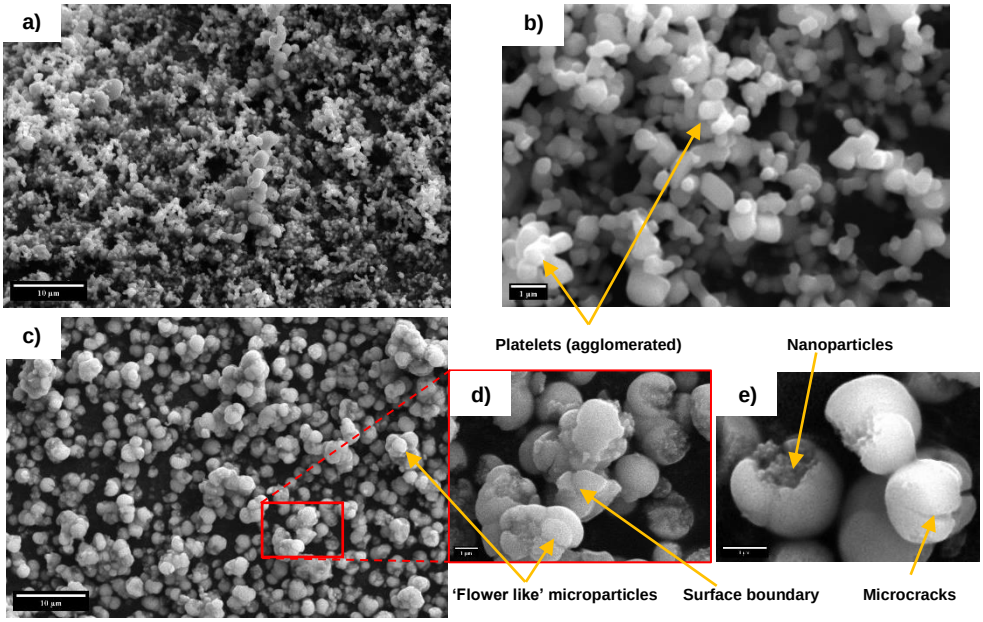


*Figure 3: SEM images of highly agglomerated rutile-anatase platelets in sample A (a, b) and pure rutile particles in sample B (c, d, e). Images (a, c) were taken at x2000 magnification, WD 17mm and SS 47, and images (b, d) are at x10,000 magnification with WD 13mm (b) and WD 17mm (d) and SS 50, zooming in at the red section. x20,000 magnification image (e) emphasises the nanoparticles and microcracks of sample B (WD 13mm, SS 45). All images have been optimised in contrast and brightness using ImageJ software[2].*

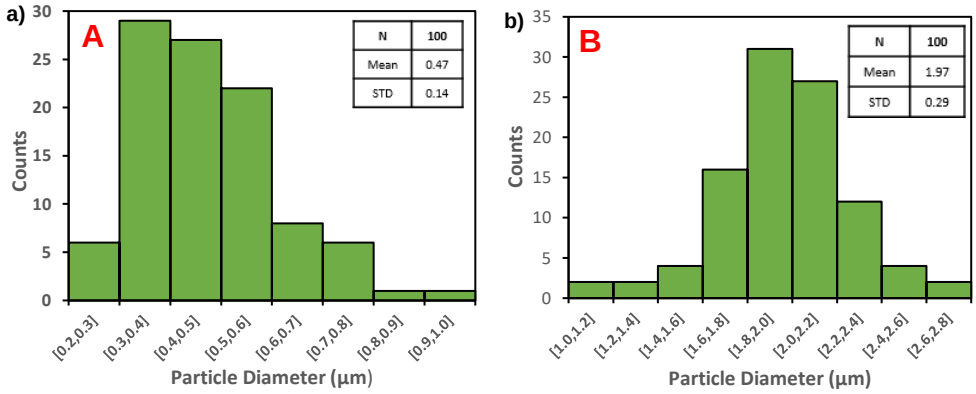


*Figure 4: Distribution plot of 100 (N) measured diameters observed in Figure 4b platelets for sample A (a) and Figure 4c microparticles for sample B (b). Statistical analysis of these distribution plots has been included, taken from ImageJ[2].*

| ELEMENT | SAMPLE A | | | | SAMPLE B | | | |
|---|---|---|---|---|---|---|---|---|
| | Map x50 | | Map x4000 | | Map x50 | | Map x14000 | |
| | Atom % | σ (%) | Atom % | σ (%) | Atom % | σ (%) | Atom % | σ (%) |
| Ti | 8.00 | 0.15 | 7.63 | 0.12 | 7.35 | 0.15 | 9.61 | 0.23 |
| O | 42.71 | 0.30 | 41.49 | 0.26 | 39.15 | 0.30 | 42.66 | 0.47 |
| C | 49.04 | 0.07 | 50.66 | 0.06 | 53.26 | 0.07 | 47.73 | 0.10 |
| Au* | 0.26 | 0.14 | 0.23 | 0.11 | 0.25 | 0.14 | - | - |
| Ti : O ratio | 1: 5.34 | | 1 : 5.44 | | 1: 5.33 | | 1: 4.44 | |

*Table 5: Quantitative map EDX results of K-level transitions taken from the JEOL JSM-6010PLUS/LA 20kV microscope, including the atomic percentage and standard deviation (σ) for each element detected. Gold (Au) was asterisked as an M-level transition. All values were rounded to 2 decimal places, including the ratio between titanium, Ti, and oxygen, O.*

Using Figure 3 (a) and (c), it's clear that particle diameters on the surface were significantly smaller on sample A than those of B. However, the recorded measurements in Figure 4 may not represent their true individual morphological size due to the agglomeration of platelets in Figure 3(a) and clustered flower-like microparticles in (b). Ishigaki et al. mentions the agglomeration behaviour increases the surface area preserves its photocatalytic properties when calcinated, sol-gel P25 $TiO_2$ is used between 700°C and 900°C, which also changes their crystal phase from anatase to rutile as temperature increases[9,10]. It's probable that sample A followed a similar process, calcinated around 700°C to sinter and coalesce to induce bonding between phases, making it ideal for surface coating to prevent bacterial damage[11]. As seen in sample B in Figure 3(d) and (e), these spherical microparticles were formed by their inner nanoparticles but with poor resolution, it raised uncertainty about their exact morphology and nucleating behaviour. While higher magnifications on SEM could be achieved, TEM information at near-atomic scale would assist in

understanding the underlying nucleation and growth of the resulting microparticles. Map EDX confirmed Ti and O were present amongst the platelets and particles seen in Figure 3, with relative atomic percentages seen in Table 5. Using atomic percentages provided a more direct chemical stoichiometry and ratio between these two elements, which averaged to 1 : 5.14, much higher than the known 1: 2 ratio in $TiO_2$ despite ZAF corrections. Part of the reason for this is due to the nature of EDX being sensitive to elements with contrasting atomic numbers, by means, O could absorb X-ray characteristic energy emitted from Ti when electron collision with high voltage electrons occurred. Across both map and point EDX (see appendix), carbon (C) and gold (Au) were recognised, but not associated with the samples themselves because of the SEM setup - carbon backing tape to mount the samples and gold to coat them, since the samples are both non-conductive.

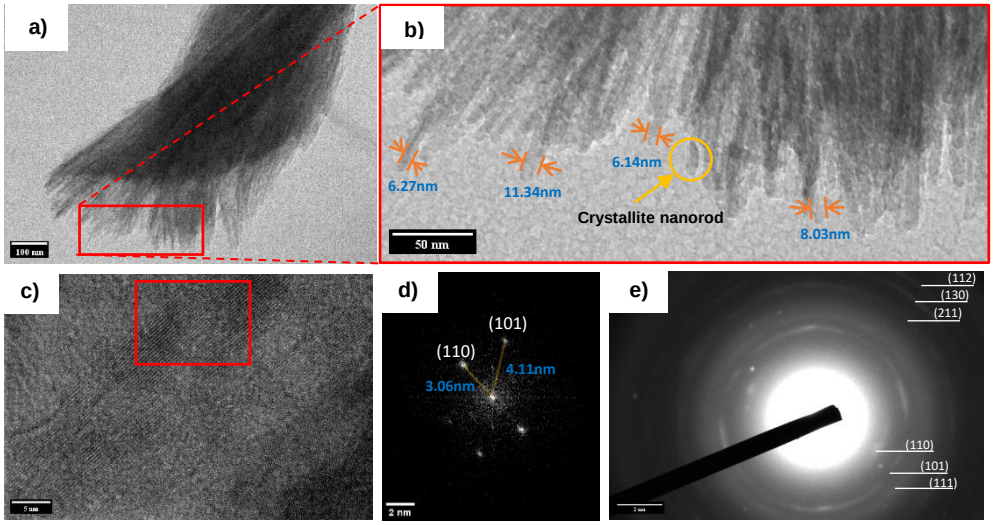


*Figure 6: TEM images of rutile $TiO_2$ sample B, taken using the JEOL JEM-2100PLUS 200 kV microscope. (a) x20000 image showing slight radial growth in the sample. (b) Cropped x50000 magnification image showing crystallites of varied thickness and (c) x600000 magnification of the atomic lattices of rutile $TiO_2$ of sample B. (d) Diffraction pattern of the region boxed in (c) which (110) and (101) were present**, and (e) SADP of various planes involved within the sample. All images have been optimised and measured (to 2 decimal places) using ImageJ[2].*

TEM images displayed certainty that sample B was indeed pure rutile $TiO_2$, being comparable to its XRD pattern. For example, the diffraction pattern in Figure 6(d) which was calculated by taking the reciprocal of 4.11nm to record 2.43 Å, close to the (111) plane's referred d-spacing value of 2.49 Å[7]. Inspection of Figure 6 (a) shows some curvature of these elongated nanorods from a nucleating centre, inferring the growth of such shape is time-dependant. Franklyn P.J et al confirmed this, as there was exponential correlation with respect to time using $TiCl_4$ under hydrothermal synthesis to transform anatase to rutile nanoparticles to rutile nanorods

– with the latter completely formed after 2 days of thorough mixing, leading to spherical microparticles[12]. Therefore, its deemed that alkaline conditions, time and quality of mixing are important factors to control the nucleation and growth of $TiO_2$ nanorods to form spherical microparticles. Nucleating such shapes are known to increase light trapping in dye sensitised solar cells (DSSC's), which improves their overall efficiency[13].

## Further Work

Performing TEM on sample A can further help understand the undirected agglomeration of platelets, as well as confirming the presence of anatase. By taking diffraction patterns of lattice-visible TEM images, the (011) characteristic plane of anatase may be identified by its' d-spacing value, given it had the highest intensity of the visible anatase peaks in Figure 1. With regards to agglomeration, zooming towards intersecting nanocrystals can potentially provide information about the bonding tendency of coherent crystal planes and how calcinated temperatures enhance a driving force for such growth to occur. In addition, using Raman spectroscopy on both $TiO_2$ samples can distinguish between the rutile and anatase polymorphs. Anatase is less symmetric which makes it more polarizable, thus intensity peaks should arise at a lower Raman shift, alongside the expected rutile peaks particularly in sample A[14].

## Conclusion

This experiment successfully characterised unknown powders A and B progressively as much as possible using XRD, SEM, EDX and TEM. It was identified that both samples were derived of anatase $TiO_2$ which transformed into rutile using different syntheses and conditions. Sample A showed 95.6wt.% rutile and 4.4wt.% anatase $TiO_2$ platelets with high agglomeration behaviour to increase its surface area for self-cleaning coatings on surfaces. This sample was likely sol-gel processed and calcinated above 700°C. For sample B, the combination of high pH ($TiCl_4$) and thorough mixing time above 2 days under hydrothermal synthesis proved to be key factors to control nucleation and growth of 100% rutile $TiO_2$ nanorods to form flower-like microparticles, which can improve efficiency in dye sensitised solar cells. It was justified that extensive time periods were necessary to permit a nucleating centre and grow radially. However, using further research such as Raman spectroscopy can help investigate between these 2 polymorphs' polarisations to discover why rutile is favoured in such applications over anatase, beyond just crystal symmetry.

## References


[1] Y. Leng, Materials Characterization: Introduction to Microscopic and *Spectroscopic Methods :Second Edition* **2013**, 1.

[2] J. Schindelin, I. Arganda-Carreras, E. Frise, V. Kaynig, M. Longair, T. Pietzsch, S. Preibisch, C. Rueden, S. Saalfeld, B. Schmid, J. Y. Tinevez, D. J. White, V. Hartenstein, K. Eliceiri, P. Tomancak, A. Cardona, Nat Methods **2012**, 9, 676.

[3] "Match! - Phase Analysis using Powder Diffraction," can be found under https://www.crystalimpact.com/match/, **2024.**

[4] "OriginLab - Origin and OriginPro - Data Analysis and Graphing Software," can be found under https://www.originlab.com/, **2024.**

[5] J. Zemann, Acta Crystallogr **1965**, 18, 139.

[6] B. M. Horn, C. F. Schwerdtfeger, E. P. Meagher, Z. KriBtallogr Bd, M. Horn, Bd **1972**, 136, 273.

[7] E. P. Meagher, G. A. Lager, **1979**.

[8] "XRD: Powder Diffraction (Scherrer Equation) - YouTube," can be found under https://www.youtube.com/watch?v=IqBtT108E5g, **2022.**

[9] T. Ishigaki, Y. Nakada, N. Tarutani, T. Uchikoshi, Y. Tsujimoto, M. Isobe, H. Ogata, C. Zhang, D. Hao, R Soc Open Sci **2020**, 7, DOI 10.1098/RSOS.191539.

[10] S. Akrami, M. Watanabe, T. H. Ling, T. Ishihara, M. Arita, M. Fuji, K. Edalati, Appl Catal B **2021**, 298, DOI 10.1016/J.APCATB.2021.120566.

[11] "How Photocatalysis works with $TiO_2$ - YouTube," can be found under https://www.youtube.com/watch?v=6PIPXIyL_ms, **2020.**

[12] P. J. Franklyn, D. C. Levendis, N. J. Coville, M. Maaza, South African Journal of Chemistry **2007**, 60, 71.

[13] X. Zhang, L. Chen, H. Pan, Z. Bao, X. Zhou, Thin Solid Films **2014**, 573, 107.

[14] J. Xu, J. Huang, S. Zhang, Z. Hong, F. Huang, Mater Res Bull **2020**, 121, 110617.


*The introductory paragraph was optimised and condensed using ChatGPT.

**Values displayed in Figure 6(d) are in reciprocal space; the ImageJ version used does not allow a reciprocal scale bar.

## Appendix

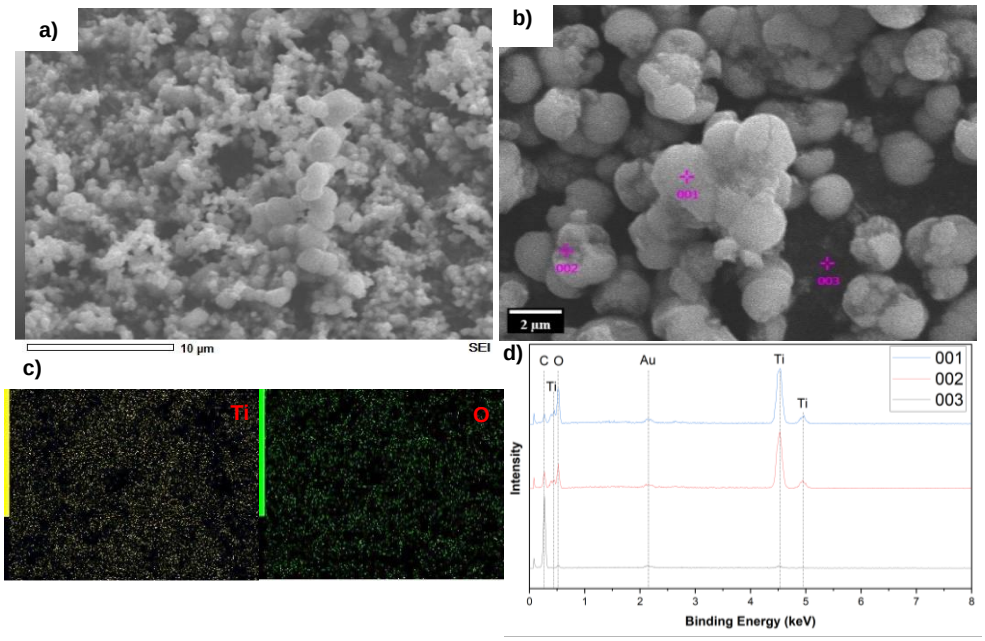


*Figure 7: SEM images for rutile-anatase sample A (a) x4000 magnification and pure rutile sample B (b), x7000 magnification using the JEOL JSM-6010PLUS/LA 20kV microscope. (c) is the elemental distribution mapping of titanium and oxygen (Ti and O respectively) within platelets of (a), and (d) shows point EDX graphs acknowledging the elements involved in (d) using points 1,2 and 3. These qualitative results comply with XRD from Figure 1.*

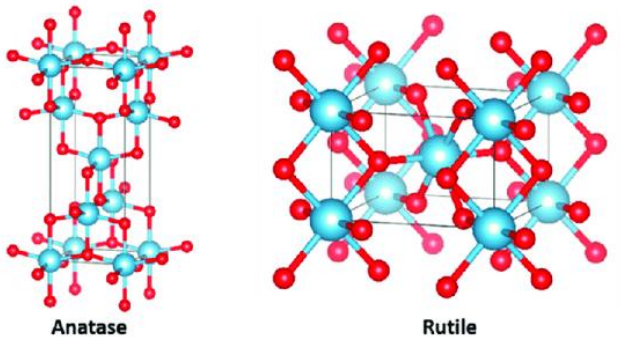


*Figure 8: Crystal unit cells of anatase and rutile $TiO_2$.*